

# Supernova remnant candidates from the Parkes 2.4-GHz survey

A. R. Duncan,<sup>1</sup> R. T. Stewart,<sup>2</sup> R. F. Haynes<sup>2</sup> and K. L. Jones<sup>1</sup>

<sup>1</sup>Physics Department, The University of Queensland, Queensland 4072, Australia

<sup>2</sup>Australia Telescope National Facility, CSIRO, PO Box 76, Epping, NSW 2121, Australia

Accepted 1996 August 21. Received 1996 August 19; in original form 1996 June 3

## ABSTRACT

25 supernova remnant (SNR) candidates are presented from the recent Parkes 2.4-GHz survey of the southern Galactic plane. Their angular diameters range from approximately 16 arcmin to 18°. Polarized emission is also detected from some of these candidates. The inclusion of these objects in current SNR catalogues will raise the number of large SNRs (diameters  $\geq 20$  arcmin) in the longitude range  $270^\circ \leq l \leq 360^\circ$  to a value comparable to that of the northern Galactic plane ( $0^\circ \leq l \leq 90^\circ$ ). An excess of SNR candidates around longitudes of  $310^\circ$ – $330^\circ$  is noted, suggesting that these objects, which are mainly of large angular diameter (greater than  $2^\circ$ ), may form part of a nearby ‘cluster’ of remnants. Comparisons with the 4.85-GHz PMN survey are also given. Pulsar associations are considered, although only one possible candidate has been found.

**Key words:** magnetic fields – polarization – supernova remnants – Galaxy: structure.

## 1 INTRODUCTION

The recent Parkes 2.4-GHz radio continuum survey (Duncan et al. 1995, hereafter referred to as Paper I) has provided high-quality images of the emission along the southern Galactic plane. This paper presents a catalogue of supernova remnant (SNR) candidates identified from the survey. Following on from the preliminary list of candidates given in Paper I, the SNR candidates presented here are the result of a more detailed examination of the 2.4-GHz survey images, the 4.85-GHz Parkes–MIT–NRAO (PMN) survey images (providing twice the resolution, but lacking emission on scalesizes of the order of 40 arcmin and larger), and *IRAS* 60- $\mu$ m infrared images. Additionally, the polarimetric images from the survey are now complete, and we examine the SNR candidates for any associated linearly polarized emission.

A total of 25 candidate remnants are presented, ranging in diameter from approximately 16 arcmin to 18°. The inclusion of these objects in future SNR catalogues will significantly increase the number of SNRs in this size range over the southern plane. Improving the representation of this type of SNR in such catalogues is a matter of importance because such remnants, which often lie at high latitudes, can provide a method for studying interstellar medium (ISM) density gradients over the southern plane, while the improvement in basic SNR statistics over this section of the Galaxy will provide stronger constraints on detailed models

of the ISM. Furthermore, the late evolution of SNRs in the low-density environments high off the plane may differ considerably from that of remnants in high-density areas close to the plane.

## 2 THE 2.4-GHz SURVEY

The Parkes 2.4-GHz survey (Paper I) is a sensitive, polarimetric, radio continuum survey of the southern Galactic plane.

The survey was carried out with the Parkes 64-m radio telescope and covers  $127^\circ$  of Galactic longitude,  $238^\circ \leq l \leq 5^\circ$ , with a latitude range of  $|b| \leq 5^\circ$  (more than this over some longitudes). The resolution of the images is 10.4 arcmin and the rms noise is approximately 17 mJy beam  $\text{area}^{-1}$  for the total-power images, and 10 mJy beam  $\text{area}^{-1}$  for the polarized intensity data. Note that this corresponds to a surface brightness sensitivity of  $4 \times 10^{-23} \text{ W m}^{-2} \text{ Hz}^{-1} \text{ sr}^{-1}$  for the total-power images at 1.0 GHz in unconfused regions (assuming a spectral index of  $\alpha = 0.5$  where  $S \propto \lambda^\alpha$ ).

In addition to the SNR candidates, the survey reveals a large amount of structure and detail in the plane emission, including a considerable number of low surface brightness loops and spurs which may be the faint vestiges of ancient SNRs.

Full details of the survey, including the total-power images, are given in Paper I. The polarization results from the survey will be published soon.

### 3 SELECTION CRITERIA

The survey has proven to be a fruitful source of SNR candidates, over a wide range of angular sizes. Details of all candidates presented in the following sections are listed in Table 1. Those presented here are based mainly on the preliminary list given in Paper I; however, careful examination of the survey images has led to some additions, and a more detailed comparison with other surveys has resulted in the removal of some candidates. Slight revisions to the central coordinates of several objects have also been made.

The criteria for selecting an object as an SNR candidate will now be briefly described.

#### 3.1 Size and morphology

First, the candidate had either to exhibit a shell-like structure, perhaps with a bi-annular (Manchester 1987) or barrel-shaped (Kesteven & Caswell 1987) morphology, or to appear noticeably extended and in an unconfused region. As the resolution of the 2.4-GHz survey images is 10.4 arcmin, this condition limits the angular sizes of the SNR candidates to a minimum of 15 to 20 arcmin (approximately 1.5 to 2.0 times the image resolution).

#### 3.2 Infrared flux

In addition to constraints on the size and morphology of the source, candidate remnants had to display little or no evidence of a thermal origin. This latter criterion was checked by examining the *IRAS* 60- $\mu$ m images (Beichman et al. 1988) surrounding each of the candidates, and applying the selection conditions given by Broadbent, Osborne & Haslam (1989) and Fürst, Reich & Sofue (1987). Candidates from the list given in Paper I that we have subsequently determined to be thermal are listed in Section 5.3.

#### 3.3 The PMN images

Images from the 4.85-GHz PMN survey (Wright et al. 1994) in the vicinity of the Galactic plane were also examined. Although the PMN data reduction processes removed large-scale structure from their images (scalesizes of the order of 40 arcmin and larger), the increased resolution and good sensitivity of the PMN images proved valuable in clarifying the nature of SNR candidates and further investigating their morphology. It should be emphasized, however, that the missing large-scale structure will produce incorrect flux densities for objects of large angular size.

**Table 1.** List of the SNR candidates identified from the survey, listing approximate sizes and other parameters. Integrated and peak fluxes are quoted for a frequency of 2.4 GHz. If integrated fluxes are not estimated, flags denote the reason(s) for this. Note that two sources (marked with an N in the *Flux* columns) were discovered by examining the 4.85-GHz PMN survey images, and have not been observed at 2.4 GHz. C – Severe confusion with bright sources. I – Incomplete coverage of the candidate in the 2.4-GHz survey. N – The source was not observed at 2.4 GHz.

<i>Centre Coordinates</i>	<i>Angular Diameter</i>	<i>Peak Flux (Jy beam<sup>-1</sup>)</i>	<i>Integrated Flux (Jy)</i>	<i>Morphology</i>
G280.5-1.0	55 × 70	0.50	5 ± 1	shell
G281.2+0.0	35 × 60	1.3	8.6 ± 1.0	bi-annular
G288.8-6.3	1°5	N	N	shell
G289.4-2.6	20 × 30	0.60	1.7 ± 0.3	filled?
G291.1+1.7	≈ 25	0.38	≈ 1.5	?
G299.3-1.5	35	1.3	6.8 ± 0.5	shell
G304+0	8°5	0.77	C	shell
G304+2	≈ 3°	0.23	C	shell?
G309.8-2.6	15 × 35	1.0	3.9 ± 1.0	?
G310.6-2.0	45	0.74	11 ± 3	bi-annular?
G310.5-3.5	2°7 × 3°5	0.35	(see text)	shell
G312.5-3.0	22	0.84	1.9 ± 0.2	shell
G312.7+3.5	1°3 × 1°7	0.35	9.1 ± 1.3	filled?
G315.1+2.7	2°5 × 3°2	0.55	19 ± 3	shell
G319.3+3.5	2° × 3°	0.38	I	bi-annular?
G321.3-3.8	1°3 × 1°8	0.62	11.1 ± 1.5	shell
G325+0	18°	C,I	C,I	shell
G332.0-3.2	2°5	0.6?	C	shell
G332.5-5.6	≈ 30	N	N	?
G333+1	≈ 6°	0.3?	C	shell
G343.0-6.0	4°	0.75	I	shell
G353.3-1.1	≈ 1°	0.57?	C	shell
G356.2+4.4	22	1.1	3.0 ± 0.3	shell
G358.0+3.8	30	0.40	2.4 ± 0.4	bi-annular
G4.8+6.2	16	0.89	1.3 ± 0.2	shell

Indeed, careful examination of the PMN images alone is a good way of searching for SNR candidates – especially those of smaller angular size (diameters  $\lesssim 30$  arcmin). Even some of the larger candidates identified from the Parkes 2.4-GHz survey can be detected on the PMN images. The large candidates (diameters  $\gtrsim 2^\circ$ ) most easily detected in the PMN survey are invariably edge-brightened shells with reasonably sharp boundaries, and appear on the images as a series of faint extended sources (this is the result of the spatial filtering of the PMN images).

As an example of this detection technique, one of the small SNR candidates examined in Section 5.1 and one of the large candidates from Section 5.2 were identified entirely from the PMN maps. These candidates, G332.5 – 5.6 and G288.8 – 6.3 (see Sections 5.1.8 and 5.2.1, respectively), were found as conspicuous areas of faint, extended emission on PMN images close to the plane. Note that the positions of these remnants place them outside the area covered by the 2.4-GHz survey. We include both these objects in our list of new SNR candidates (Table 1), and will also consider them for follow-up investigations.

#### 4 KNOWN SNRs

Before discussing the new SNR candidates, it should be noted that the Parkes 2.4-GHz survey contains a large amount of new information relating to known SNRs.

For example, Fig. 1 shows an image of the supernova remnant G350.0 – 1.8 (Milne & Dickel 1970), seen from the 2.4-GHz survey. The SNR was given this designation because only the bright, northern arc was detected in previous observations. Clearly, we are imaging the entire shell of this remnant, and suggest that this object should be (more correctly) designated G350.0 – 2.0.

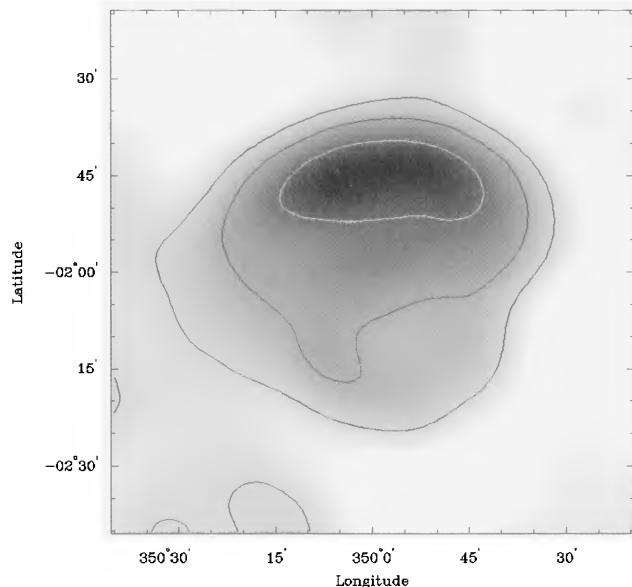


**Figure 1.** The 2.4-GHz survey image of the known SNR G350.0 – 1.8 (see Section 4). Note that this image reveals the full extent of the shell, which appears centred on  $b = -2^\circ$ . The contour levels used are 280, 700 and 1500 mJy beam area $^{-1}$ .

#### 5 NEW SNR CANDIDATES

It is convenient at this point to break the list of SNR candidates presented in Table 1 into two classes, ‘small’ and ‘large’, based on their angular diameter. Any candidate with an angular size less than approximately  $2^\circ$  we will consider ‘small’, and anything larger than this will be classed as ‘large’.

Separating the SNR candidates into these two groups also serves to emphasize the fact that the larger candidates may represent a different class of remnant. All but one of the large remnants appear as edge-brightened and often filamentary arcs, mainly detected towards high latitudes, away from the bright, confusing emission of the Galactic plane. Because of the symmetry inherent in these arcs, the structures often appear as large, partial rings or ellipses. If these structures are indeed SNRs then they must be both large and old; certainly in the radiative phase, and almost at the point of merging with the ISM. The effects of these large remnant candidates on the statistics of SNRs over the southern plane will be considered further in Section 6.

We will examine the small candidates in the following section, and the large candidates in Section 5.2.

##### 5.1 Small candidates

We will now examine the small SNR candidates from the 2.4-GHz survey. A total of 13 such candidates are presented here. The corresponding images from the PMN survey are also included where their higher resolution reveals additional structure within the candidate.

###### 5.1.1 G280.5 – 1.0

This candidate is seen as an area of emission, some  $55 \times 70$  arcmin $^2$  in size, with a central minimum. The candidate is

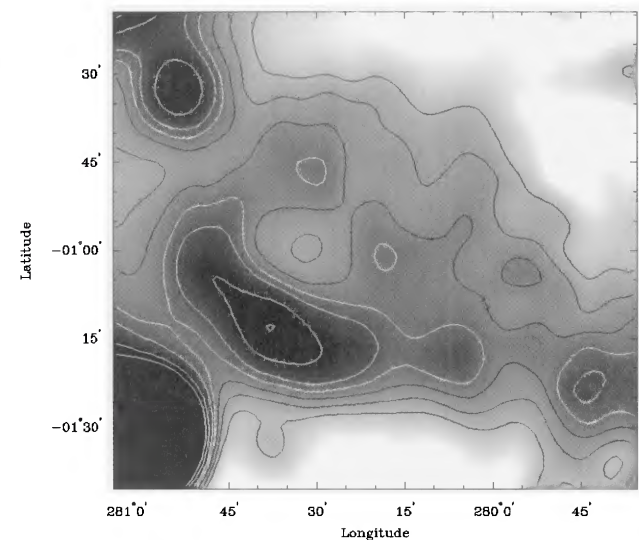


**Figure 2.** G280.5 – 1.0 (see Section 5.1.1) as seen by the Parkes 2.4-GHz survey. The bright source in the south-east corner of the image is the thermal complex G281.013 – 1.528. Contour levels are 100, 150, 200, 250, 300, 400 and 500 mJy beam area $^{-1}$ .

brightest on its south-eastern limb, which is the only section of the candidate visible on the PMN images. The 2.4-GHz survey image is shown in Fig. 2. The bright source complex in the south-eastern corner of the figure is the thermal complex G281.013 – 1.528 (Caswell & Haynes 1987).

There is a considerable amount of polarization in the vicinity of the object, but this polarized emission shows little evidence of being associated with the candidate. The integrated flux at 2.4 GHz is  $5 \pm 1$  Jy.

### 5.1.2 G281.2 + 0.0

This SNR candidate, very close to G280.5 – 1.0, is a distinctly elliptical object approximately  $35 \times 60$  arcmin<sup>2</sup> in size and exhibiting intensity peaks near the ends of the major axis. As is also the case of G280.5 – 1.0, the peak flux density of this candidate is to the south-east. The 2.4-GHz

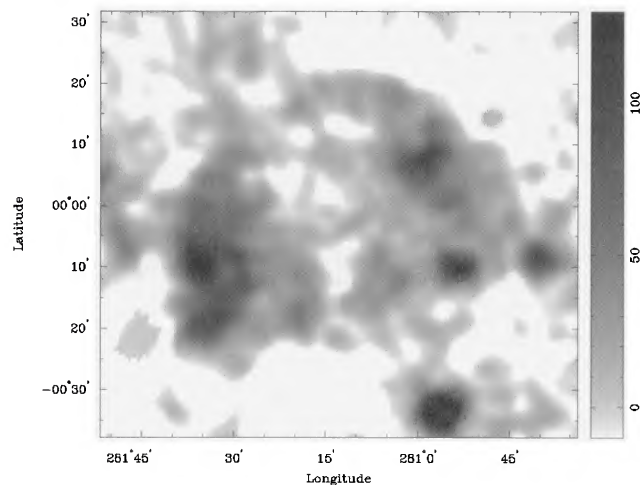
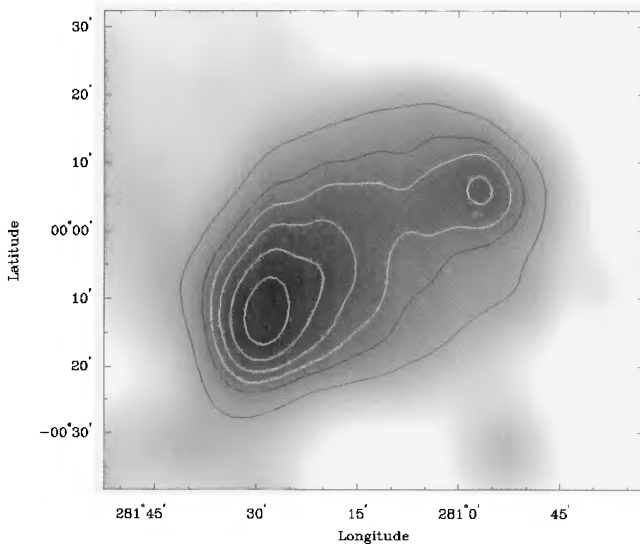


**Figure 3.** G281.2 + 0.0 (see Section 5.1.2), showing images from (a) the 2.4-GHz survey, and (b) the 4.85-GHz PMN survey. The contour levels used in (a) are 600, 800, 900, 1000, 1100 and 1200 mJy beam area<sup>-1</sup>. The grey-scale wedge used in (b) is labelled in units of mJy beam area<sup>-1</sup>.

survey image is shown in Fig. 3(a), with the corresponding 4.85-GHz PMN image in Fig. 3(b). The PMN survey resolves the candidate into a bi-annular structure, showing two clear limbs of emission.

As mentioned in Section 5.1.1, there is a large amount of polarized emission present in this region of the Galactic plane (also encompassing the remnant G279.0 + 1.1). The polarization vectors and distribution of polarized intensities imply that much of this polarization is not associated with the remnant candidates discussed here. The integrated flux is  $8.6 \pm 1.0$  Jy at 2.4 GHz.

### 5.1.3 G289.4 – 2.6

This object, pictured in Fig. 4, appears as a smooth patch of emission some  $20 \times 30$  arcmin<sup>2</sup> in size. The candidate lies close to a bright, compact source identified from the PMN catalogue as PMN J1047 – 6217.

No polarization is detected from this candidate, and examination of the PMN images does not reveal any further structural detail. The 2.4-GHz integrated flux is  $1.7 \pm 0.3$  Jy.

### 5.1.4 G291.1 + 1.7

This object is seen in Fig. 5 as the easternmost of two patches of emission. Examination of 60- $\mu$ m *IRAS* images clearly shows the western feature, identified as G290.4 + 1.6 (see Section 5.3), to be thermal. Although some thermal emission can be seen in the vicinity of G291.1 + 1.7, this does not appear bright enough to account for the intensity of the radio feature detected in the 2.4-GHz survey. Whether this object is an SNR or not is still unclear. No polarization was detected at 2.4 GHz.

Although somewhat uncertain because of the plateau of emission apparently joining G291.1 + 1.7 and G290.4 + 1.6, the integrated flux at 2.4 GHz is estimated to be  $\approx 1.5$  Jy.

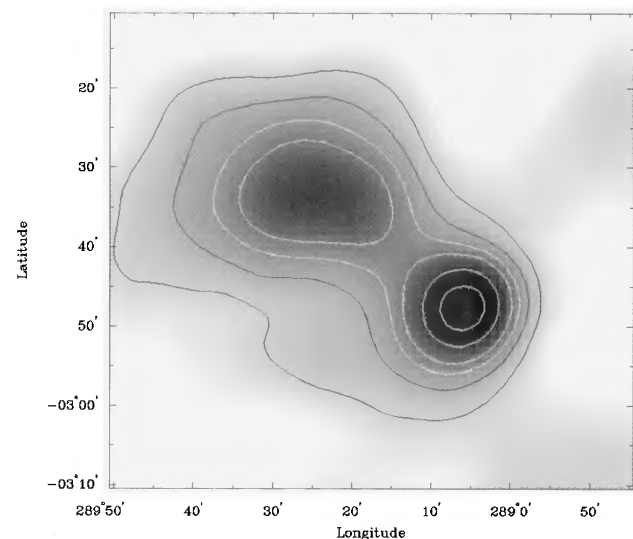


**Figure 4.** G289.4 – 2.6 (see Section 5.1.3) as seen by the Parkes 2.4-GHz survey. The bright, compact source is identified in the PMN catalogue as PMN J1047 – 6217. Contour levels are 100, 200, 300, 400, 600 and 800 mJy beam area<sup>-1</sup>.

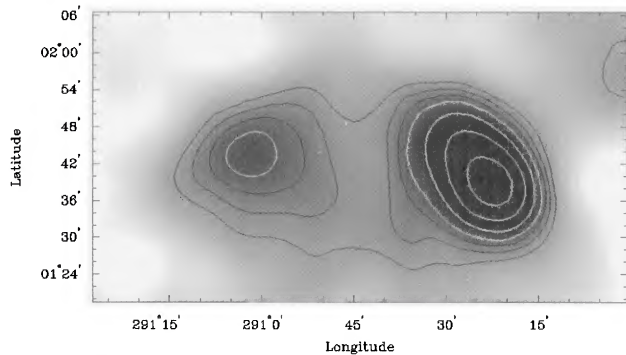


**Figure 5.** G291.1 + 1.7 and G290.4 + 1.6 at a frequency of 2.4 GHz (see Sections 5.1.4 and 5.3, respectively). The eastern source appears non-thermal, while the brighter, western source is thermal. Contour levels are 200, 250, 300, 350, 450, 600 and 800 mJy beam area<sup>-1</sup>.

### 5.1.5 G299.3 – 1.5

The candidate G299.3 – 1.5, pictured at 2.4 GHz in Fig. 6(a), has an approximately circular appearance, some 35 arcmin in diameter, with the emission concentrated towards the north-west (i.e. towards the bright plane emission). Again, no polarization was detected from this object.

The PMN 4.85-GHz image shows interesting structure in this source (Fig. 6b), resolving the SNR candidate into a series of broad filaments of emission. These filaments appear concentrated towards the brighter, north-western side of the candidate – in agreement with the 2.4-GHz brightness distribution. The integrated flux density is  $6.8 \pm 0.5$  Jy at 2.4 GHz.

### 5.1.6 G309.8 – 2.6 and G310.6 – 2.0

These two candidate SNRs are shown together in Fig. 7. The more westerly of the two, G309.8 – 2.6, appears as an elongated area of enhanced emission some  $15 \times 35$  arcmin<sup>2</sup> in size, with a brightening towards the south-west. G310.6 – 2.0 is large, with a roughly circular boundary, approximately 45 arcmin in diameter. This latter remnant exhibits a very broad, low-contrast, bi-annular appearance. Note that a pulsar, B1358 – 63, is seen coincident with the G310.6 – 2.0 candidate. The position of the pulsar is marked on Fig. 7 by a circle and cross, and is further discussed in Section 6.3.

Inspection of the PMN images does not show any great improvement in structural detail for either of these candidates, although it reveals that the brightness enhancement on the south-western side of G309.8 – 2.6 is an extended feature and not a compact source (i.e. not a chance alignment of an extragalactic object).

Infrared images show there is some thermal emission present around the larger G310.6 – 2.0 candidate, but this does not appear to be of sufficient intensity or extent to account for the radio emission of the candidate.

Interestingly, these objects lie within the shell emission of one of the large SNR candidates (G310.5 – 3.5: Section 5.2.3) responsible for much of the diffuse emission seen in Fig. 7. The whole of G310.5 – 3.5 is shown in Fig. 16(a) (later), with G309.8 – 2.6 and G310.6 – 2.0 visible on the

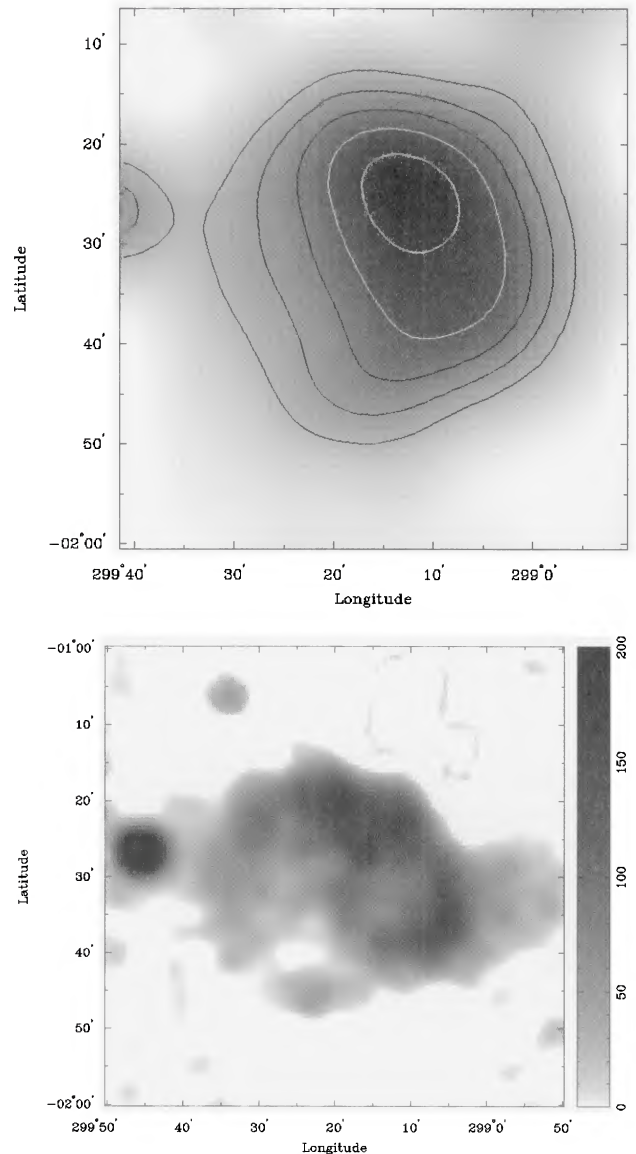


**Figure 6.** G299.3 – 1.5 (see Section 5.1.5), as seen by both (a) the 2.4-GHz survey, and (b) the 4.85-GHz PMN survey. The contour levels used in (a) are 400, 600, 800, 1000 and 1200 mJy beam area<sup>-1</sup>. The grey-scale wedge used in (b) is labelled in units of mJy beam area<sup>-1</sup>.

northern side of the shell. This raises the following question: are these two smaller objects SNR candidates in their own right, or simply regions of enhanced shell emission within the larger G310.5 – 3.5 candidate? They are certainly much brighter than the rest of the emission associated with the G310.5 – 3.5 shell; however, their confinement to this shell must be viewed as somewhat suspicious.

Some bright areas of polarization are seen coincident with these SNR candidates, and these are shown in Fig. 16(b), along with the polarization over the larger G310.5 – 3.5 candidate. The characteristics of this polarization suggest that it is probably produced by the larger G310.5 – 3.5 shell, rather than either of these smaller candidates. This implies that these latter objects may be unrelated to the larger G310.5 – 3.5.

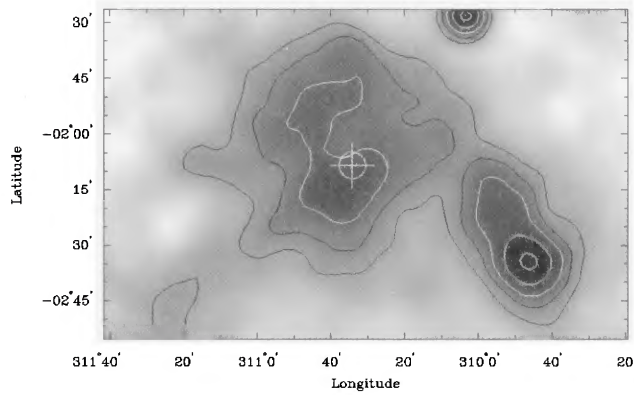


**Figure 7.** G309.8 – 2.6 and G310.6 – 2.0 at a frequency of 2.4 GHz (see Section 5.1.6). The position of the pulsar B1358 – 63 is marked by a circle and cross. Contour levels are 300, 450, 600, 800 and 1000 mJy beam area<sup>-1</sup>.

A clarification of the nature of these two SNR candidates and their relationship to the larger G310.5 – 3.5 shell (if any) must await further, higher resolution observations.

Approximate integrated flux densities for the candidates are  $4 \pm 1$  Jy for G309.8 – 2.6 and  $11 \pm 3$  Jy for G310.6 – 2.0. Note that the uncertainty in these values is increased by their superposition on the emission of the large candidate G310.5 – 3.5.

#### 5.1.7 G312.5 – 3.0

Appearing in Fig. 8 as a circular, extended source with smooth and almost uniform surface brightness, this object is a good SNR candidate. Additionally, the PMN images resolve this candidate into a beautiful, barrel-shaped, ring structure with the highest surface brightnesses detected towards the western edge. This barrel morphology makes the object's identity as a SNR even more probable.

No polarization is seen in our 2.4-GHz images associated with this SNR candidate. The 2.4-GHz flux density is  $1.9 \pm 0.2$  Jy.

#### 5.1.8 G332.5 – 5.6

During examination of the PMN images near the Galactic plane, G332.5 – 5.6 was seen as a conspicuous region of filamentary emission (see Fig. 9), approximately 30 arcmin in diameter. Three straight filaments can be discerned, aligned in a similar direction. Note that the PMN survey's filtering of large-scale structure has probably removed most of the emission from G332.5 – 5.6. This remnant candidate is unusual in that it was identified exclusively from the PMN survey – the 2.4-GHz survey did not image this region. Hence we cannot determine the integrated flux or investigate the polarization of this SNR candidate.

Although the appearance of this object does not conform to a general SNR morphology, its angular extent and proximity to the plane, coupled with the lack of any infrared emission, make it a possible candidate. As such, we have included it in our list of candidates, and will include it in any further investigations. This object was discovered on PMN image J1630 – 50.

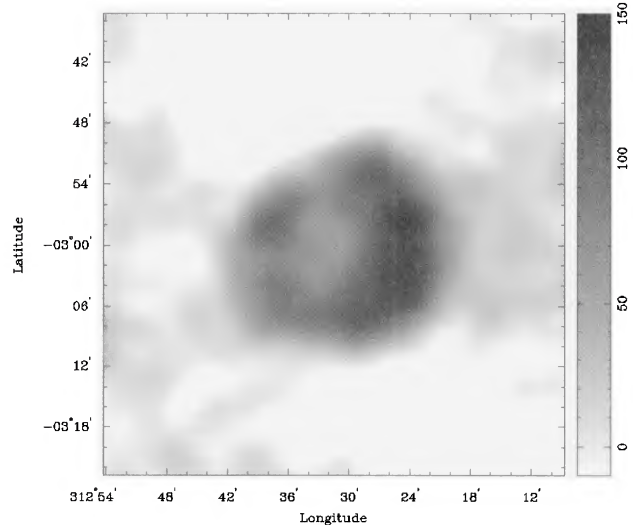
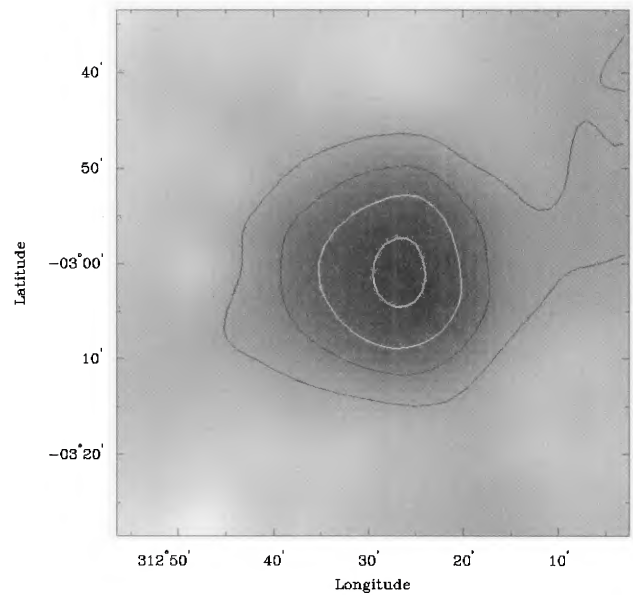


**Figure 8.** G312.5 – 3.0 (see Section 5.1.7), as seen by both (a) the 2.4-GHz survey, and (b) the 4.85-GHz PMN survey. The contour levels used in (a) are 200, 400, 600 and 800 mJy beam area<sup>-1</sup>. The grey-scale wedge used in (b) is labelled in units of mJy beam area<sup>-1</sup>.

#### 5.1.9 G353.3 – 1.1

Appearing as a small, loop-like object with a mottled appearance, this candidate may be a section of an edge-brightened SNR shell. The 2.4-GHz image is shown in Fig. 10. Comparison with 60- $\mu$ m *IRAS* images shows that the object is not composed of thermal emission, and the loop-like morphology suggests an SNR interpretation. Note that much of the north side of the loop may be hidden by bright H II complexes.

No polarization was detected from this loop. Because of the confusion of this object with nearby H II regions and thermal emission, it is not possible to determine the integrated flux of this candidate reliably.

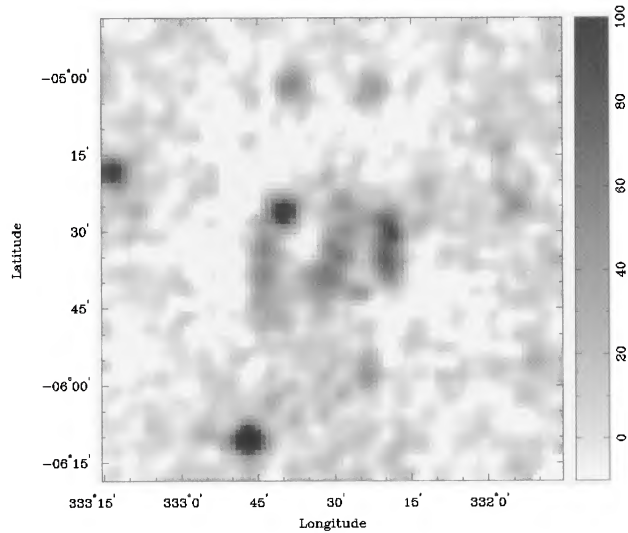


**Figure 9.** G332.5 – 5.6 (see Section 5.1.8). This image was identified as an SNR candidate after examination of the 4.85-GHz PMN images in the vicinity of the Galactic plane. The grey-scale wedge is labelled in units of  $\text{mJy beam area}^{-1}$ .

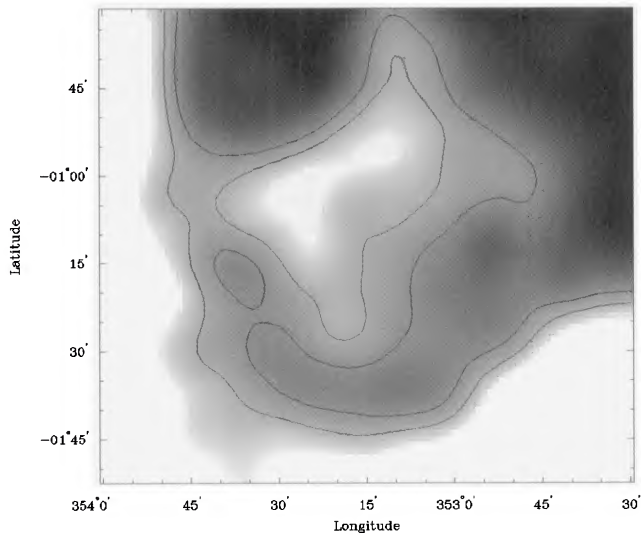


**Figure 10.** G353.3 – 1.1 from the Parkes 2.4-GHz survey (see Section 5.1.9). Contour levels are 150 and 300  $\text{mJy beam area}^{-1}$ .

#### 5.1.10 G356.2 + 4.4

A small and almost circular region of emission (Fig. 11), this candidate is quite similar to G312.5 – 3.0 (see Fig. 8 and Section 5.1.7) in both size and appearance. The increased resolution of the 4.85-GHz PMN image reveals this object as a well-defined ring, exhibiting large variations in surface brightness. Note that, as this candidate is positioned near the edge of the PMN survey ‘zenith strip’, some parts of the emission to the south-west of the object are missing at the higher frequency. The pulsar B1717 – 29 appears near G356.2 + 4.4 – its position is marked on Fig. 11(a) by a circle and cross. The possibility of an association is discussed in Section 6.3.

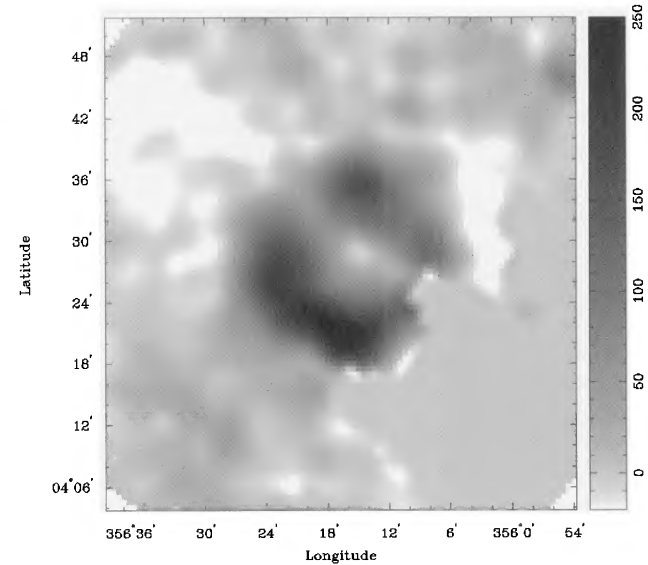
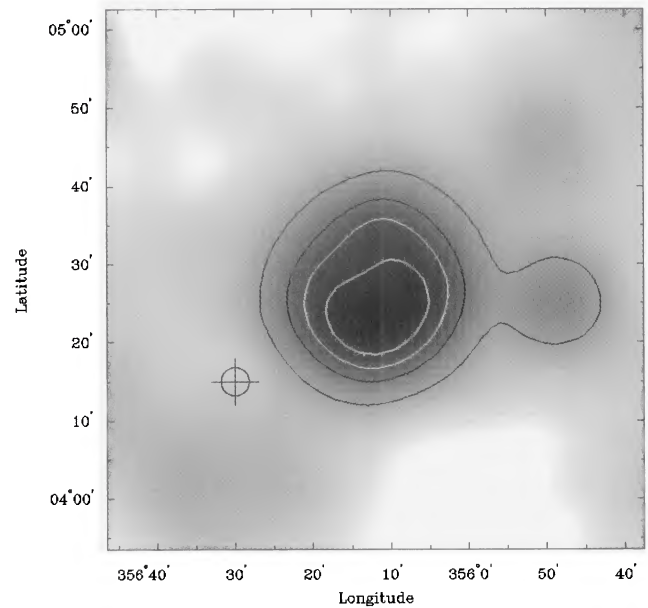


**Figure 11.** G356.2 + 4.4 at frequencies of (a) 2.4 GHz and (b) 4.85 GHz (see Section 5.1.10). Note that part of the 4.85-GHz image is missing, because of the object’s proximity to the PMN survey’s ‘zenith strip’. The position of the pulsar B1717 – 29 is marked in (a) by a circle and cross. The contour levels used in (a) are 230, 500, 700 and 900  $\text{mJy beam area}^{-1}$ . The grey-scale wedge used in (b) is labelled in units of  $\text{mJy beam area}^{-1}$ .

No polarization from this object is evident. The integrated flux at 2.4 GHz is  $3.0 \pm 0.3$  Jy.

#### 5.1.11 G358.0 + 3.8

This candidate appears morphologically similar to the SNR G350.0 – 1.8 (Fig. 1), with one arc dominating the emission.

The integrated flux is  $2.4 \pm 0.4$  Jy at 2.4 GHz, and as such this object has the lowest surface brightness of all of the small candidates presented in this section. No polarization was detected associated with the object.

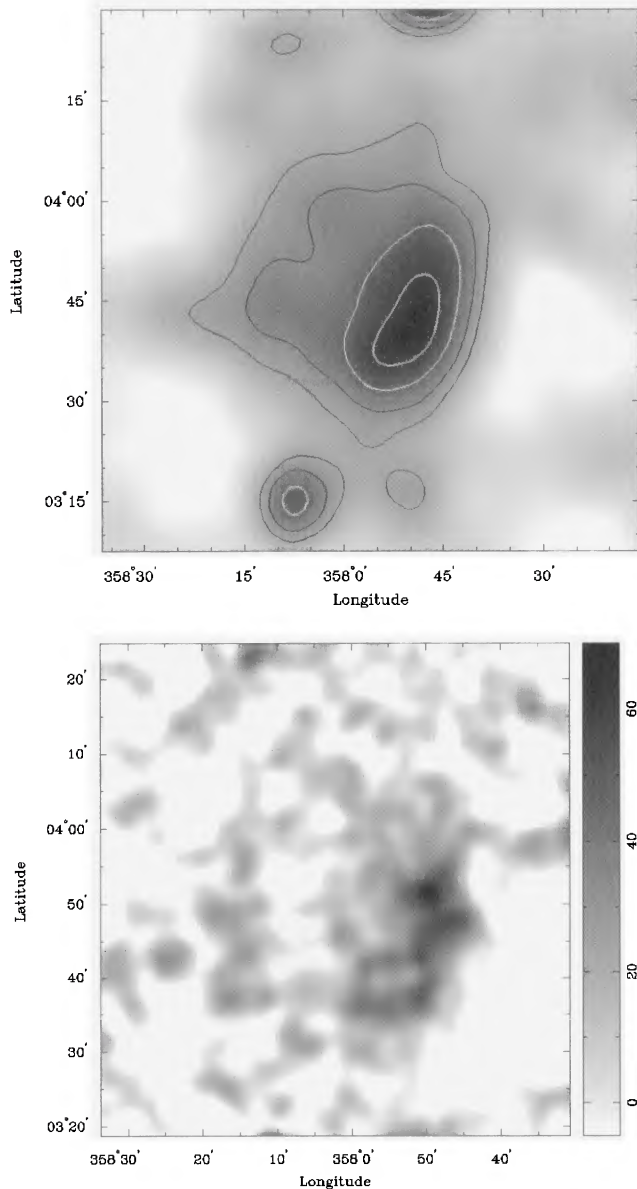


**Figure 12.** Images from (a) the Parkes 2.4-GHz survey and (b) the 4.85-GHz PMN survey of the SNR candidate G358.0+3.8 (see Section 5.1.11). Contour levels seen in (a) are 140, 200, 280 and 360 mJy beam area<sup>-1</sup>. The grey-scale wedge used in (b) is labelled in units of mJy beam area<sup>-1</sup>.

A 4.85-GHz image of this object was obtained from the PMN survey, and is shown in Fig. 12 along with our 2.4-GHz image. At the higher frequency (and with the smaller beam) much of the emission appears absent, although a faint eastern arc can be detected. The PMN image also reveals interesting structure within the bright, western arc. Note that 60- $\mu$ m images suggest that there may be some thermal component to this object.

#### 5.1.12 G4.8+6.2

This SNR candidate is pictured in Fig. 13 at a frequency of 2.4 GHz, showing both the (a) total-power and (b) polarized

intensity images. Appearing as a smooth patch of emission approximately 20 arcmin across, this object lies very close to Kepler's SNR (G4.5+6.8; Dickel et al. 1988).

This candidate appears brightly polarized (see Fig. 13b) with an almost constant orientation of the polarization vectors across the source. A mean fractional polarization of up to 25 per cent is determined from our 2.4-GHz data.

The 4.85-GHz image (Fig. 13c), obtained from the PMN survey, resolves the candidate into a well-defined ring. The morphology and presence of polarized emission make it highly likely that this object is a supernova remnant.

The integrated 2.4-GHz flux density is  $1.3 \pm 0.2$  Jy.

## 5.2 Large candidates

In this section, images showing the large SNR candidates from the Parkes 2.4-GHz survey are presented and briefly described.

### 5.2.1 G288.8-6.3

During examination of the PMN images in the vicinity of the Galactic plane, G288.8-6.3 was seen as a conspicuous ring of mottled emission (see Fig. 14), approximately 1.5° in diameter. Note that the insensitivity of the PMN survey to large-scale structure has probably removed most of the emission from G288.8-6.3. This remnant candidate is unusual in that it was identified exclusively from the PMN survey – the 2.4-GHz survey did not image this region. Hence we cannot determine the integrated flux or investigate the polarization of this SNR candidate.

The appearance of the candidate is similar to that of other large, filamentary SNR candidates, as seen by the PMN survey, suggesting that it is indeed an SNR candidate. We have included this object in our list of candidates, and will also include it in any follow-up investigations. This object was discovered on PMN image J1030-65.

### 5.2.2 G304+0 and G304+2

One of the most prominent rings identified from the survey images is centred near G304+0 (Fig. 15), and is some 8.5° across. This object is seen as a series of ring arc segments, symmetric about the central point. The arcs are mainly seen at higher latitudes, away from the bright, confusing emission close to the plane. Seemingly situated within the boundary of this remnant is yet another possible SNR candidate: G304+2. Approximately 3° in diameter, the southerly half of this structure is obscured by the Galactic plane, and hence the object appears as a semicircle, rather similar in form to the larger G304+0 which surrounds it. The arcs of emission forming this smaller object appear to have a correspondingly smaller radius of curvature than those of G304+0, and hence it is possible that they form part of an independent remnant.

No polarized emission is seen associated with either of these candidates. Unfortunately, integrated flux values for either of these remnant candidates are impossible to estimate accurately, because of confusion with bright Galactic sources. The peak flux density over the G304+0 ring is 770 mJy beam area<sup>-1</sup>, seen on the south-eastern section of the shell.

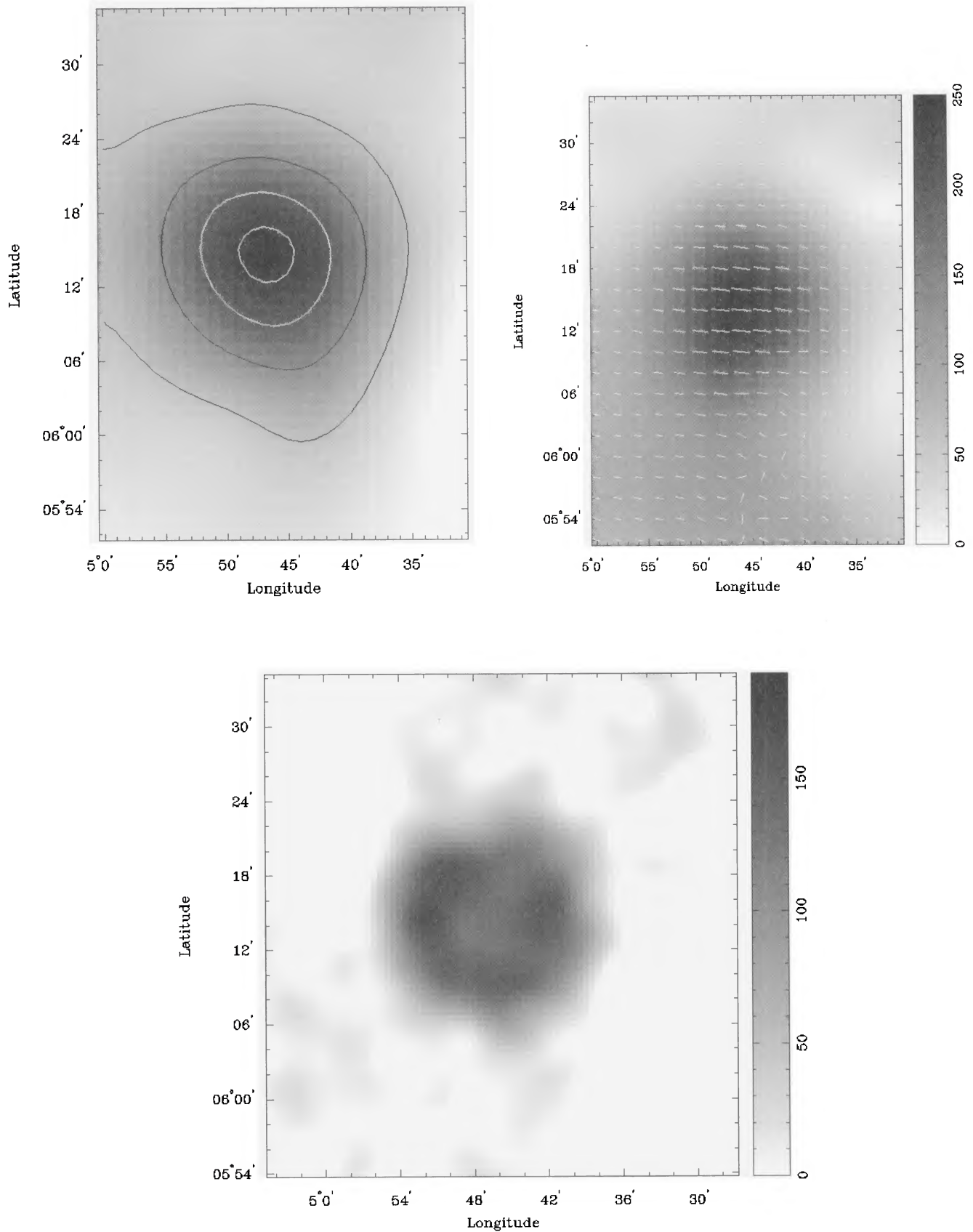


**Figure 13.** The 2.4-GHz (a) total-power and (b) polarized intensity images of G4.8 + 6.2 (see Section 5.1.12). The 4.85-GHz PMN survey image is shown in (c). The contour levels used in (a) are 230, 500, 720 and 860 mJy beam area<sup>-1</sup>. The grey-scale wedges seen in (b) and (c) are labelled in units of mJy beam area<sup>-1</sup>. The vectors seen in (b) indicate the orientation of the magnetic vector of the received radiation at each point, with a length proportional to the polarized intensity (the maximum polarized intensity is 235 mJy beam area<sup>-1</sup>).

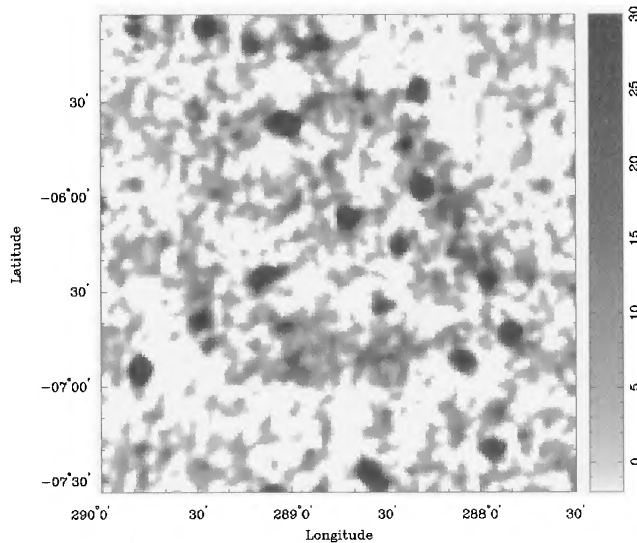


**Figure 14.** G288.8 – 6.3 (see Section 5.2.1). This image was identified as an SNR candidate after examination of the 4.85-GHz PMN images in the vicinity of the Galactic plane. The grey-scale wedge is labelled in units of  $\text{mJy beam area}^{-1}$ .

### 5.2.3 G310.5 – 3.5

Another large SNR candidate is G310.5 – 3.5, seen in Fig. 16. The 2.4-GHz total-power image is shown in Fig. 16(a) and the polarized intensity image is seen in (b). In total-power, this object appears as a faint, broad and diffuse shell structure (unlike many of the other large candidates, the shells of which appear more filamentary), some  $2^{\circ}.7 \times 3^{\circ}.5$  in size. The bright emission to the north of the shell is from two small SNR candidates: G309.8 – 2.6 and G310.6 – 2.0 (see Fig. 7 and Section 5.1.6). The integrated flux at 2.4 GHz for G310.5 – 3.5 is  $34 \pm 5$  Jy, including the bright, northern shell emission, or  $19 \pm 5$  Jy if the bright, northern objects are subtracted.

Some bright and patchy regions of polarized intensity are seen across the shell, rising up to  $120 \text{ mJy beam area}^{-1}$  ( $\approx 40$  per cent fractional polarization). The vector directions shown in Fig. 16(b) correspond to the magnetic vector of the received radiation. In general these vectors appear circumferential around the shell, indicating both that the rotation measures (RMs) across the object are quite low ( $\lesssim 30 \text{ rad m}^{-2}$ ) and that a large-scale magnetic field structure exists within the object.

### 5.2.4 G312.7 + 3.5

The total-power image of G312.7 + 3.5 is seen in Fig. 17(a) as a roughly circular region of emission, centrally filled, approximately  $1^{\circ}.5$  in diameter. Very little variation in surface brightness is seen across the object. The integrated flux at 2.4 GHz is  $9.1 \pm 1.3$  Jy. Note that the bright regions in the south-western corner of Fig. 17(a) are H II regions close to the plane (we are looking almost tangentially to the Centaurus arm at this longitude).

The polarized intensity image is seen in Fig. 17(b). The vector directions correspond to the magnetic vector of the received radiation, with a length proportional to the polar-

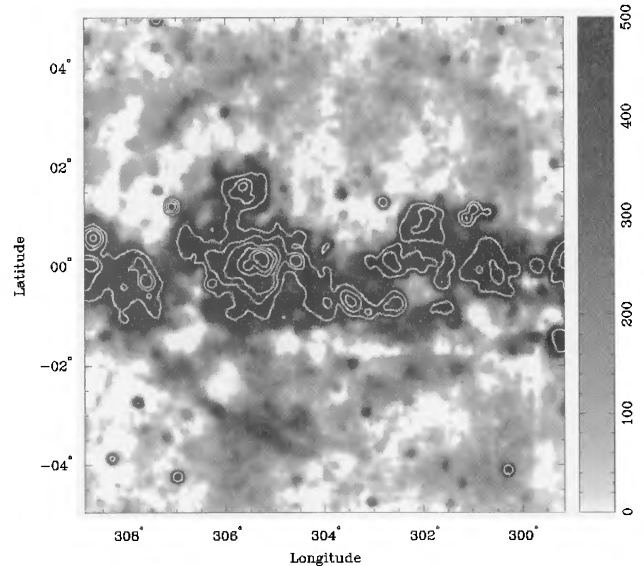


**Figure 15.** G304 + 0 and G304 + 2 at a frequency of 2.4 GHz (see Section 5.2.2). The bright emission seen near  $b = 0^{\circ}$  is dominated by H II regions. The SNR candidates are seen as large, faint arcs of emission at latitudes of between  $2^{\circ}$  and  $4^{\circ}$  from the plane. Contour levels are 0.8, 2, 4, 10, 20 and  $40 \text{ Jy beam area}^{-1}$ .

ized intensity. A bright, extended patch of polarized emission appears coincident with the candidate, although this may be unrelated. Sensitive, higher resolution observations are required to answer this question.

### 5.2.5 G315.1 + 2.7

The total-power image of this candidate appears in Fig. 17(a) as an edge-brightened, broken ‘ring’ or elliptical structure,  $2^{\circ}.5 \times 3^{\circ}.2$  in size. Note that the shell exhibits large variations in definition and surface brightness along its length. The brightest and most clearly defined section of the remnant shell is to the east, with a peak flux density of  $550 \text{ mJy beam area}^{-1}$ . The integrated flux is  $19 \pm 3$  Jy. Note that the 4.85-GHz PMN survey shows the sharp boundary of this object beautifully, although we do not show the PMN image here (because it does not provide any further information on morphology or structure of the candidate).

Polarization across the candidate is shown in Fig. 17(b), with several bright patches of polarized emission seen within or around the total-power candidate. Again, the vector orientations correspond to the magnetic vector of the received radiation. The distribution of polarized intensity implies that some of this polarization is indeed associated with the SNR candidate.

### 5.2.6 G319.3 + 3.5

The arcs of emission forming this object, which is seen in Fig. 18, are embedded within the western limb of the large SNR candidate G325 + 0 (discussed in Section 5.2.8). The appearance of these arcs is such that they are most probably enhancements in the shell of the larger SNR candidate, rather than a separate object.

No polarized emission was convincingly detected from these structures. We consider this an unlikely candidate.

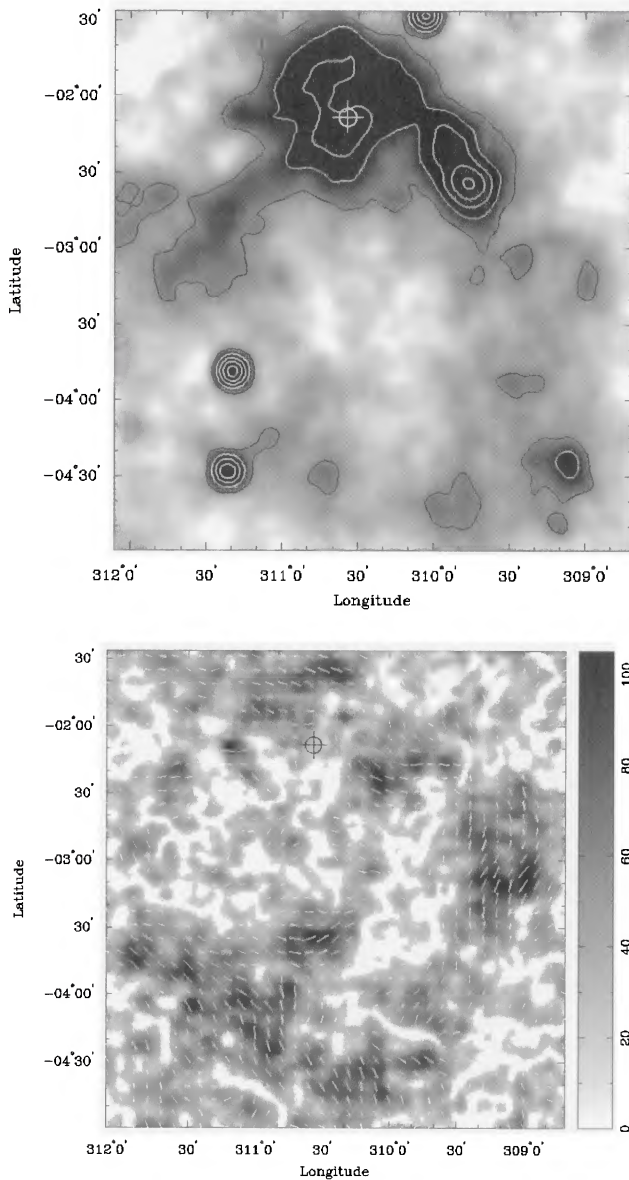


**Figure 16.** (a) The total-power image and (b) the polarized intensity image of G310.5 – 3.5, as seen in the Parkes 2.4-GHz survey (see Section 5.2.3). The bright, ‘burnt out’ regions to the north of the shell in (a) are the smaller SNR candidates G309.8 – 2.6 and G310.6 – 2.0 (see also Fig. 7). The vectors in (b) indicate the orientation of the magnetic vector of the received radiation, with a length proportional to the polarized intensity at each point (the maximum polarized intensity is  $117 \text{ mJy beam area}^{-1}$ ). The contour levels used in (a) are 200, 400, 600, 800 and  $1000 \text{ mJy beam area}^{-1}$ . The grey-scale wedge used in (b) is labelled in units of  $\text{mJy beam area}^{-1}$ .

### 5.2.7 G321.3 – 3.8

Seen in Fig. 19 at a frequency of 2.4 GHz, the SNR candidate G321.3 – 3.8 appears as an ellipse approximately  $1.3 \times 1.8$  in size. Fig. 19 shows (a) the total-power image and (b) the polarized intensity image. The north-western side of the object is much fainter and more diffuse than the south-eastern edge, which appears as a well-defined arc.

Polarized emission is detected from the bright arc, which exhibits a maximum fractional polarization of 50 per cent

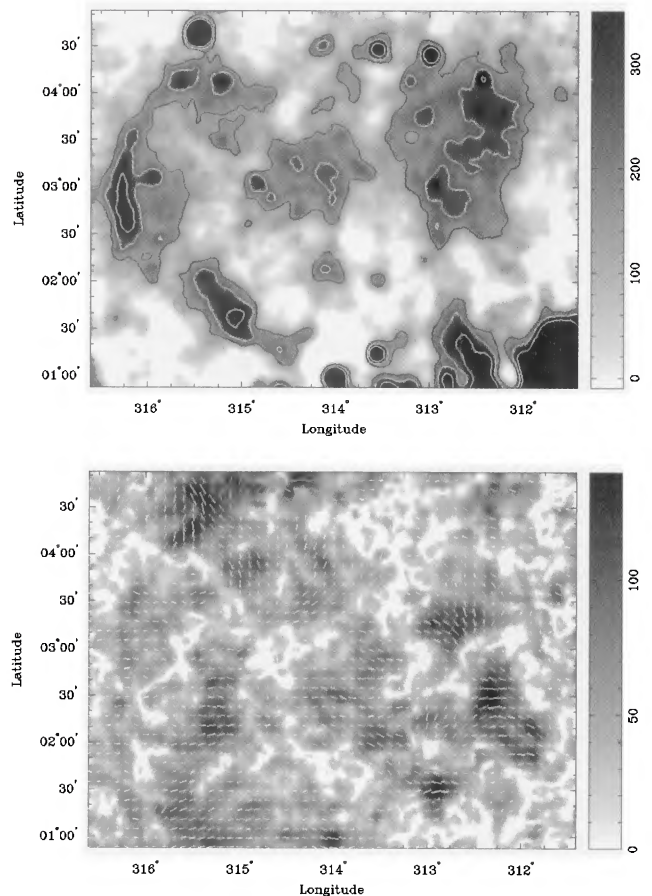


**Figure 17.** G312.7 + 3.5 and G315.1 + 2.7 (see Sections 5.2.4 and 5.2.5, respectively) from the Parkes 2.4-GHz survey, showing both (a) the total-power and (b) the polarized intensity images. The vectors in (b) indicate the orientation of the magnetic vector of the received radiation, with a length proportional to the polarized intensity at each point (the maximum polarized intensity is  $220 \text{ mJy beam area}^{-1}$ ). Bright H II complexes are seen in the south-west corner of the total-power image. The contour levels used in (a) are 150, 250 and  $400 \text{ mJy beam area}^{-1}$ . The grey-scale wedge used in (b) is labelled in units of  $\text{mJy beam area}^{-1}$ .

along its most southerly section. The vector directions do not appear oriented along the arc, which is probably the result of Faraday rotation effects. Note that an increased RM may be because the object is within or behind the large candidate G325 + 0. The integrated flux at 2.4-GHz is  $11.1 \pm 1.5 \text{ Jy}$ .

### 5.2.8 G325 + 0

The largest SNR candidate discovered from the 2.4-GHz survey is G325 + 0, shown in Fig. 20. The object is  $18^\circ$  across, although the survey has imaged the candidate in the latitude range  $|b| \leq 5^\circ$  only.

The total-power image (Fig. 20a) has been filtered to remove low spatial frequencies, on angular scalesizes of the order of  $2^\circ$  and larger. This highlights the broad ‘spur’ structures associated with the edges of the shell (Fig. 20c). However, much of the shell emission appears as part of the large-scale structure, which is particularly difficult to render in grey-scale hardcopies and hence is not shown here. Emis-

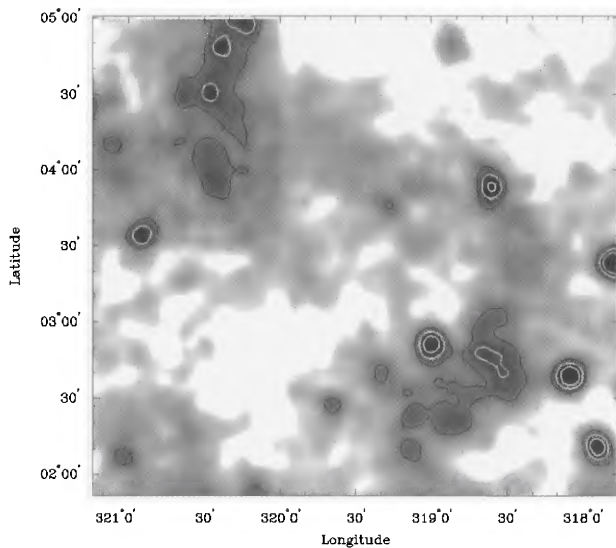


**Figure 18.** G319.3 + 3.5 at a frequency of 2.4 GHz (see Section 5.2.6). Contour levels are 200, 300 and 400 mJy beam area<sup>-1</sup>.

sion from the shell is detected over a large section of the field shown in Fig. 20, with the eastern arc spanning 6° of the radius of the object (see the sketch in Fig. 20c). Note that the candidates G319.3 + 3.5, G321.3 – 3.8 and G332.0 – 3.2 (Sections 5.2.6, 5.2.7 and 5.2.9, respectively) are also visible within Fig. 20.

A large amount of polarized emission is seen over the field (Fig. 20b), with the brightest emission seen on the northern side of the plane (up to 350 mJy beam area<sup>-1</sup>). These polarization structures are large-scale and appear very patchy. A curious ‘spur’ is also present in the polarized intensity image, extending northwards from the brightly polarized region near 329° longitude. Note that this spur, along with all of the bright polarization structure, lies within the boundary of the G325 + 0 candidate. Furthermore, the curvature of the spur matches that of the total-power shell emission, favouring an association for this structure at least. The vector orientations appear relatively constant over the brightly polarized regions.

As we have not imaged the entire object, and also because of the presence of the bright H II complexes towards low latitudes, we have not estimated the integrated flux of the candidate.

### 5.2.9 G332.0 – 3.2

Seen in Fig. 21 is the 2.4-GHz total-power image of G332.0 – 3.2. Note that this object appears superposed upon the eastern limb of the large SNR candidate G325 + 0 (discussed in Section 5.2.8). Although shaped as a recognizable ring, it is possible that this feature is associated with the G325 + 0 object, rather than emission from a separate candidate. At this time we cannot differentiate between these two possibilities.

The polarized intensity image of the region (see Fig. 20) shows emission coincident with the brightest sections of the object, with vector orientations (magnetic vector) which appear roughly circumferential.

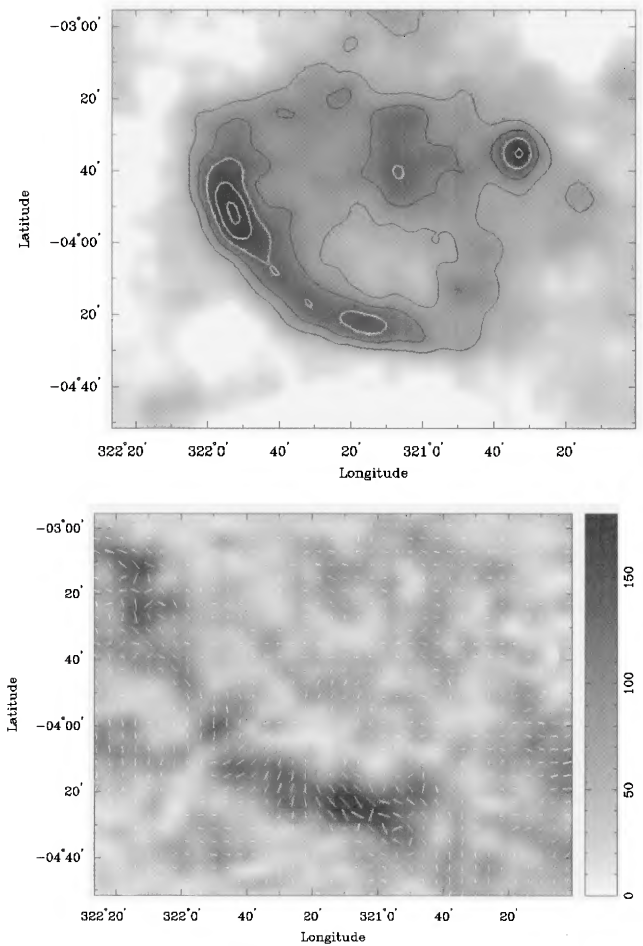


**Figure 19.** The (a) total-power and (b) polarized intensity images of G321.3 – 3.8 at a frequency of 2.4 GHz (see Section 5.2.7). The vectors shown in (b) indicate the orientation of the magnetic vector of the received radiation. The vector length is proportional to the polarized intensity at each point. The contour levels used in (a) are 200, 300, 400, 500 and 600 mJy beam area<sup>-1</sup>, while the grey-scale wedge used in (b) is labelled in units of mJy beam area<sup>-1</sup>.

### 5.2.10 G333 + 1

Close to the large candidate G325 + 0 lies an arc of faint emission which may be a section of an old, edge-brightened SNR shell: G333 + 1. The 2.4-GHz total-power image is shown in Fig. 22(a), along with (b) a sketch of the region, highlighting the position of the arc. Note that much of the emission associated with this candidate may be masked by the bright H II complexes at lower Galactic latitudes.

The polarized intensity image shows some emission around this area, but its distribution makes it unlikely to be associated with the total-power arc.

### 5.2.11 G343.0 – 6.0

A large ‘loop complex’ was detected within the 2.4-GHz survey, between Galactic longitudes of 339° and 345° (see Fig. 23). These structures are seen to extend towards both positive and negative Galactic latitudes, out to approximately 7° from the plane, and were commented on in Paper I. Note that the 2.4-GHz survey does not quite cover the

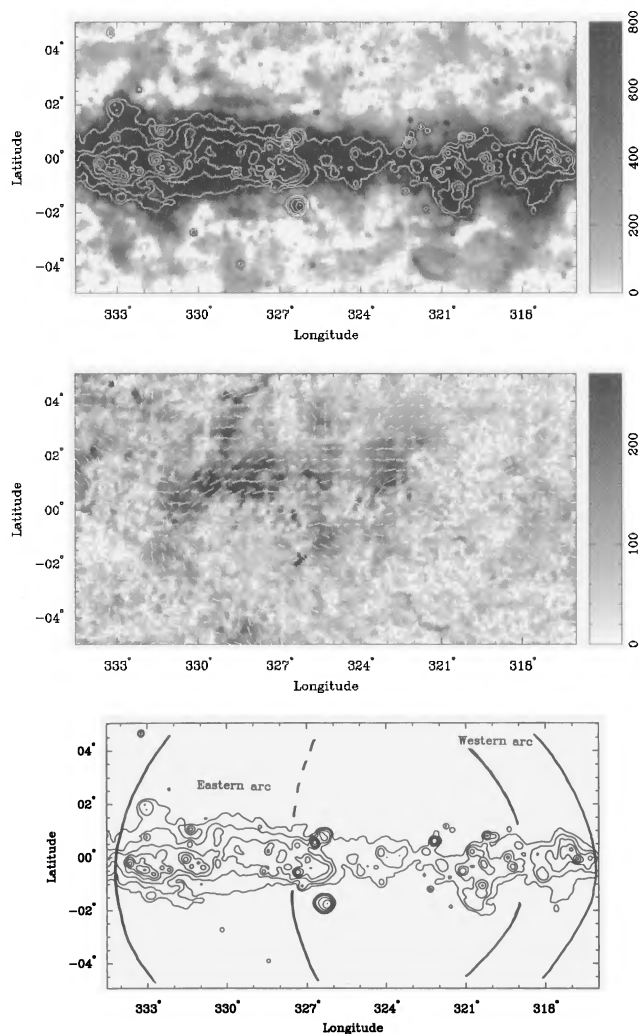


**Figure 20.** The Parkes 2.4-GHz survey image of G325 + 0 (see Section 5.2.8), showing (a) the total-power image, (b) the polarized intensity image, and (c) a sketch showing the two broad arcs of the candidate, as identified from the unfiltered data. Note that the vectors shown in (b) again indicate the magnetic vector of the received radiation, with a length proportional to the polarized intensity at each point. The contours used in (a) and (c) are at levels of 1, 2, 4, 8, 15, 30 and 60 Jy beam area<sup>-1</sup>. The grey-scale wedge used in (b) is labelled in units of mJy beam area<sup>-1</sup>.

entire structure towards negative Galactic latitudes. The bright remnant G343.1 – 2.3 (McAdam, Osborne & Parkinson 1993) also appears prominently in Fig. 23(a).

The interpretation of these structures is now somewhat clearer. The bright spurs to the north of the Galactic plane appear to be outflows of hot, ionized material, sourced from the bright H II complex G345.0 + 1.5. Optical imaging of this H II complex (also known as IC 4628) by Laval (1972) clearly shows ionized material streaming away towards northern Galactic latitudes. It is probable that the bright arcs of material towards positive latitudes, which reach up to  $b = +5^\circ$ , result from this material moving through the gravitational potential of the Galaxy and falling back towards the disc. Further ionization of the material is probably supplied by NGC 6231 and the Sco OB 1 association, which are positioned quite close to the arcs and lie at a

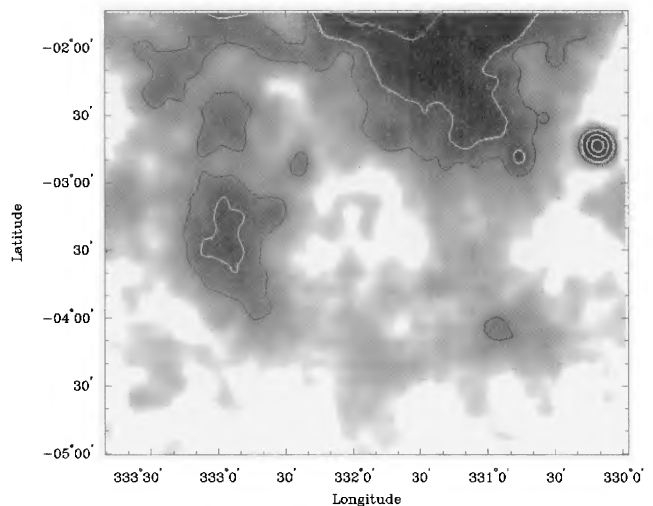


**Figure 21.** The remnant candidate G332.0 – 3.2 (see Section 5.2.9), showing the total-power image at a frequency of 2.4 GHz. The contours are at levels of 0.3, 0.5, 1.0 and 1.5 Jy beam area<sup>-1</sup>.

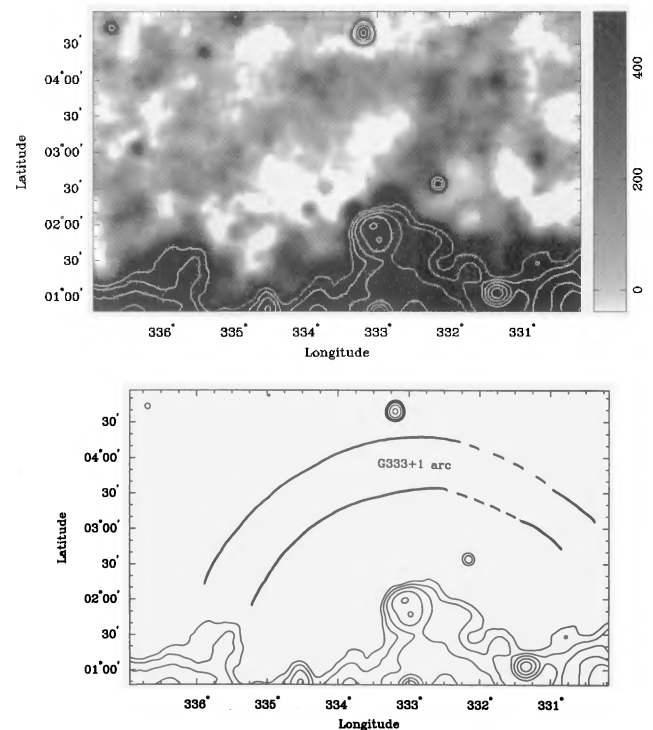


**Figure 22.** Visible section of the G333 + 1 arc at a frequency of 2.4 GHz (see Section 5.2.10), showing (a) the total-power image and (b) a sketch of the region, highlighting the arcuate structure. Contour levels are 0.7, 1.0, 1.5, 2.4, 4 and 6 Jy beam area<sup>-1</sup>.

similar distance (Perry, Hill & Christodoulou 1991). No significant polarization is detected across these structures, as expected for thermal emission. Note that the G345.0 + 1.5 complex lies at a distance of about 2 kpc (Laval 1972; Caswell & Haynes 1987).

It appears that much of the structure seen towards negative Galactic latitudes, rather than being related to the spurs on the northern side, is radio frequency emission from the

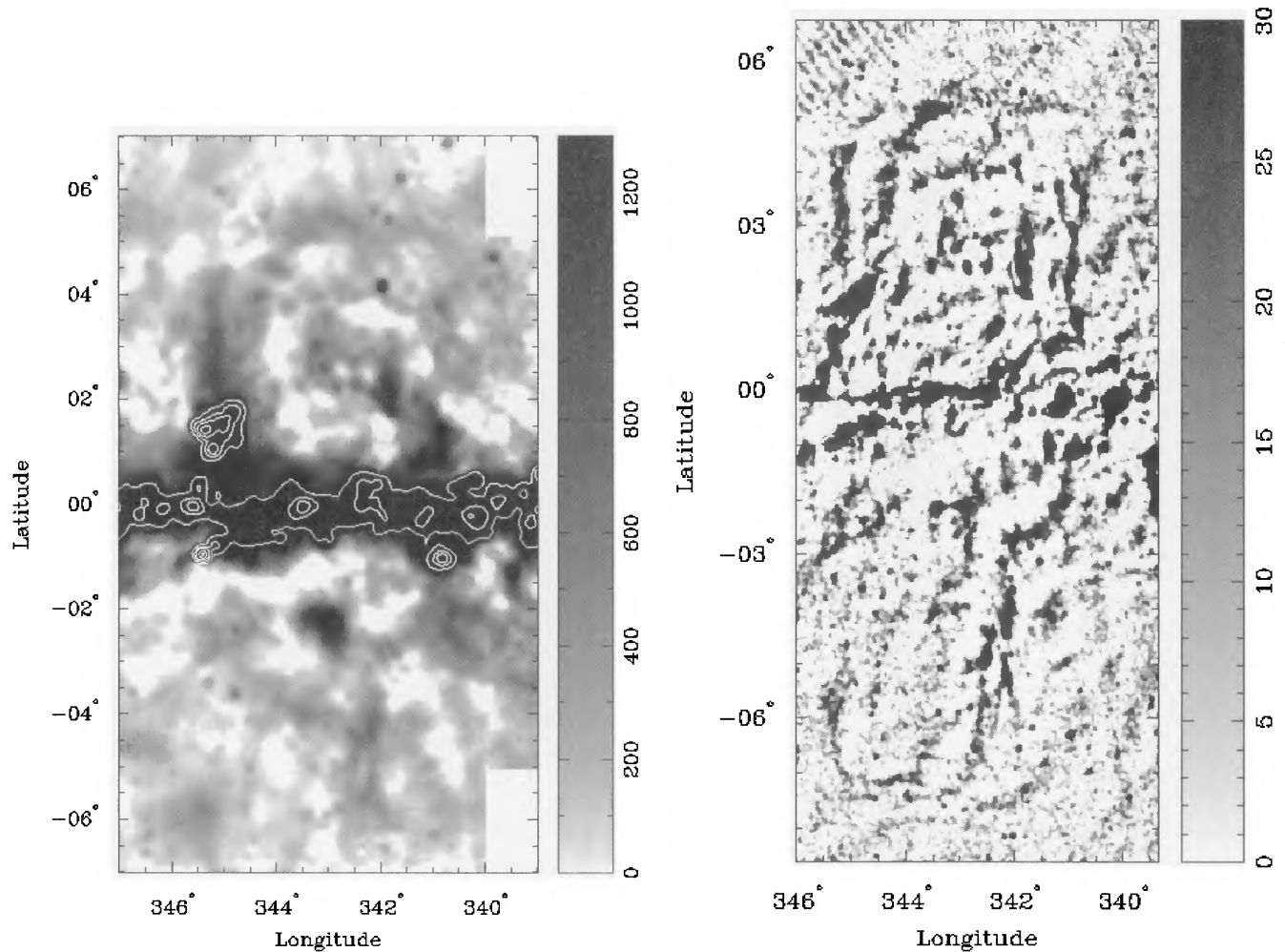


**Figure 23.** The large ‘spur complex’ about  $342^\circ$  longitude (see Section 5.2.11), as seen by both (a) the 2.4-GHz survey, and (b) the 4.85-GHz PMN survey. The SNR candidate G343.0 – 6.0 can be seen to the south of the plane, although the 2.4-GHz image does not completely cover this object. Note that the bright remnant G343.1 – 2.3 appears prominently in image (a). The contour levels used in (a) are 2, 5, 10, 20 and 30 Jy beam area $^{-1}$ . The grey-scale wedge used in (b) is labelled in units of mJy beam area $^{-1}$ .

filamentary nebula 1723 – 46 discovered by Meaburn & Rovithis (1977). Absorption spectra of several stars aligned with the nebula were obtained by Bedford, Elliott & Ramsey (1984), who found evidence for an expanding shell at a distance of  $\lesssim 200$  pc. This distance is clearly incompatible with the  $\approx 2$ -kpc value for the G345.0 + 1.5 H II complex, ruling out any association between the structures. More recently, Meaburn et al. (1991) have observed H $\alpha$  spectra over several areas of the G343.0 – 6.0 nebula, determining an expansion velocity of  $25\text{--}35$  km s $^{-1}$  and interpreting the objects as a Type II supernova evolving in the momentum-conserving phase. The weakness of the thermal emission, also investigated by Meaburn et al., in comparison with the 2.4-GHz flux densities implies that the radio emission we detect is non-thermal.

This object, centred on G343.0 – 6.0, was once catalogued as an SNR (Green 1984), but later removed from that classification (see Green 1988) chiefly because it was not detected at radio wavelengths. On this basis, we suggest that G343.0 – 6.0 should be reintroduced into future SNR catalogues.

This interpretation of the ‘spur’ structures is still uncer-

tain, awaiting observations at other radio frequencies to determine the spectral index distribution. We are in the process of obtaining both 1.4- and 4.85-GHz observations over the field for this purpose.

Finally, it should be noted that the spectral index value quoted in Paper I for a section of these spurs has now been brought into question. The uncertainty has arisen because the 1.4-GHz observations used to determine the spectral index covered only a small section of the spur structures, and an error in the setting of the ‘zero level’ has probably occurred. There is a reasonable possibility that the spectral index of the ‘spurs’ seen to the north of the plane is close to that expected for optically thin thermal emission; this will be clarified once data at other frequencies have been obtained.

### 5.3 Mistaken candidates

This section briefly discusses the SNR candidates nominated in Paper I that have subsequently been shown not to be SNRs. Images of all the objects mentioned in this section can be found within fig. 5 of Paper I.

Most of these mistaken candidates have proven to be thermal sources, and were rejected through examination of the 60- $\mu\text{m}$  *IRAS* infrared images. Specifically, G287.2 + 2.7, G290.4 + 1.6, G292.7 – 1.6, G294.3 – 3.5, G298.5 + 2.2, G309.6 + 4.0, G320.7 – 1.5, G337.5 + 1.5 and G352.6 + 2.2 are all seen to have strong, thermal counterparts.

The candidate G283.7 + 4.7 has been identified as a pair of point-like sources, probably extragalactic, confused within the large beam of the Parkes radio telescope at 2.4 GHz. The high resolution of the PMN images separates the two sources, which have catalogue designations of PMN J1038 – 5311 and J1039 – 5310.

Morphologically similar to an SNR, G294.3 – 3.5 has been shown to be a combination of a compact source (probably extragalactic) and faint H II emission. The source is designated PMN J1127 – 6505 in the 4.85-GHz PMN catalogue. The G338.5 + 2.9 candidate has also been shown not to be an SNR. The eastern side of this feature has a strong thermal component, while the remainder does not appear to form a convincing shell.

## 6 SUPERNOVA REMNANTS OVER THE SOUTHERN PLANE

### 6.1 The Parkes sample

It has long been known that SNR surveys and samples are subject to selection effects (e.g. Green 1984; Hughes, Hefland & Kahn 1984). Consequently, catalogues of SNRs (such as Green 1995) are generally biased towards the brighter and more easily identified remnants. Additionally, because of the coverage and resolution of many surveys, current catalogues greatly favour the detection of remnants towards low Galactic latitudes – within a degree or so of the plane. As a result, our current knowledge of SNRs is biased towards bright and relatively small objects residing in high-density environments.

A total of 25 SNR candidates are presented in this paper. Assuming that all of these candidates are indeed supernova remnants (with the exception of G304 + 2 and G319.3 + 3.5, which we consider to be unlikely candidates), it is of interest to examine the properties of this new sample and how it relates to current catalogues of SNRs.

Examining the catalogue of Green (1995), remnants with diameters of 20 arcmin or greater were selected and binned in 15° intervals of Galactic longitude. The resulting histogram is shown in Fig. 24(a) as a solid line. Note that in this histogram, and throughout the rest of the discussion, we will also include the recently discovered remnant G299.2 – 2.9 (Busser, Eggert & Aschenbach 1995). Discovered as part of the *ROSAT* all-sky X-ray survey, this SNR appears on the 2.4-GHz survey as a source approximately 20 arcmin in diameter, while the 4.85-GHz PMN images show a well-defined ring.

This solid line histogram seen in Fig. 24(a) shows the general form expected: a peak near the Galactic Centre and a trough near the anticentre. Note that histograms incorporating all SNRs (i.e. regardless of angular size) show a much more pronounced peak – see for example fig. 1 of Gray (1994). This is because a sample of larger remnants will contain proportionately more nearby objects (which will be distributed more isotropically, because of their prox-

imity) than will an SNR sample containing all angular sizes.

Most importantly, the histogram in Fig. 24(a) shows a clear deficiency of SNRs of large angular size (i.e. angular diameters  $\geq 20$  arcmin) over the southern plane. A similar deficiency can be seen in the solid line histogram of Fig. 24(b) which shows the longitude distribution of remnants with  $|b| \geq 2^\circ$ . Hence the problem of under-representing large, high-latitude SNRs is particularly acute over the southern Galaxy. Indeed, the total number of large remnants in the range  $0^\circ < l < 90^\circ$  (43 SNRs) is approximately twice the number known in the range  $270^\circ < l < 360^\circ$  (24 SNRs).

The dotted lines seen in Figs 24(a) and (b) show the improvement in the counts of large and high-latitude SNRs after including the candidate remnants presented in this paper (again, excluding G304 + 2 and G319.3 + 3.5). This increases the number of large-diameter remnants to a value comparable to that of the northern plane. The number of SNRs at high latitudes (over the entire Galactic plane) is also increased by about 40 per cent. Note that only 13 high-latitude remnants are known over the longitude range of the 2.4-GHz survey (Green 1995), and so the sample presented here will be more than double this number. Again comparing with the catalogue of Green (1995), the SNR candidates presented herein will increase the total number of remnants within the longitude range of the survey by approximately 26 per cent, increasing the overall catalogue size by over 12 per cent.

Examining the histograms presented in Fig. 24 shows that we have increased the central peak of the distributions slightly. However, the most interesting feature is the presence of a second peak, located around longitudes of  $310^\circ$ – $330^\circ$ . This new of the distribution appears in both Figs 24(a) and (b) at approximately the  $2\sigma$  level. It is mainly the large candidates (several degrees in diameter) that are responsible for this increase – an interesting point which will be discussed further in the next section.

### 6.2 The large candidates: a new class of remnant?

As mentioned previously, current SNR catalogues are incomplete for remnants of large angular size. The largest SNR catalogue by Green (1995) is G65.3 + 5.7, which is  $5.2 \times 4.0$  in size (Gull, Kirshner & Parker 1977). It has also been suggested that the large Galactic loops are old SNRs; an idea argued by Berkhuijsen, Haslam & Salter (1971) and one which has recently been given further support (at least for Loop I) by Egger & Aschenbach (1995). Many studies have suggested (e.g. Berkhuijsen 1986; Green 1988) that remnants with angular sizes between that of G65.3 + 5.7 (of the order of  $5^\circ$ ) and that of Loop IV, the smallest of the Galactic loops (of the order of  $40^\circ$ ), ought to exist despite their absence from current catalogues.

Many of the large SNR candidates discussed in Section 5.2 have diameters comparable to, or larger than, that of G65.3 + 5.7. Two of these in particular, G304 + 0 and G325 + 0, have diameters that lie between those of the largest catalogues SNR and the smallest of the four Galactic loops. The fact that such objects have evaded all searches until now shows just how difficult these large candidates are to detect. These large objects may ‘bridge the gap’ in diam-

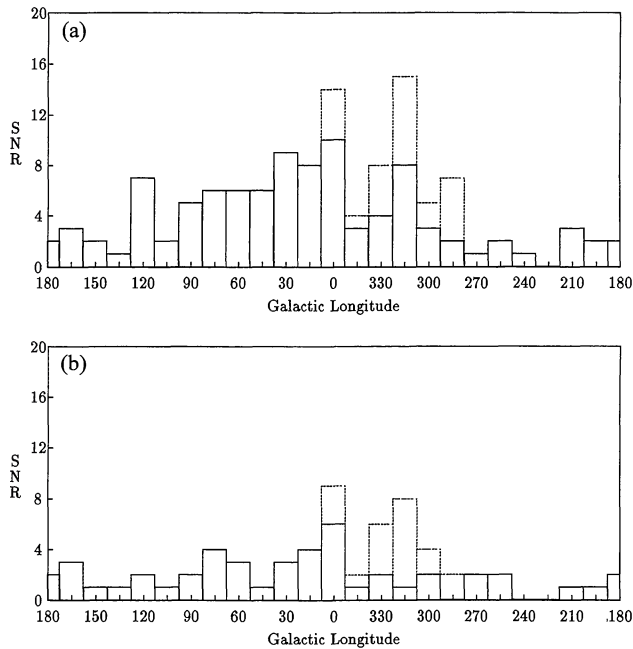


**Figure 24.** Histograms showing the number of (a) large SNRs (with diameters  $\geq 20$  arcmin) and (b) high-latitude SNRs ( $|b| \geq 2^\circ$ ) over the Galactic plane, binned in  $15^\circ$  intervals of longitude. The solid line indicates the number of known remnants (from the catalogue of Green 1995), while the dotted line shows the SNR counts after the inclusion of the candidates presented in Table 1 (excluding G304 + 2 and G319.3 + 3.5, which we consider unlikely candidates). Note the interesting peak around longitudes  $310^\circ$ – $330^\circ$  in both (a) and (b); this is discussed in Section 6.2.

eter between known SNRs and the loops, possibly adding further weight to the idea that the loops are indeed large SNRs.

Examining the catalogue of Green (1995), a total of nine remnants with angular diameters of  $2^\circ$  or larger are listed. In Section 5.2 we present 10 new SNR candidates with diameters exceeding this value, approximately doubling the number known. Many of these shells appear as broken ring-segments or partial rings, indicating that they must be old and therefore of large linear size. Indeed, many appear almost at the point of merging with the ISM. Consequently, such objects offer a unique insight into the behaviour of large remnants, near the end of their evolution, which are probably evolving in low-density environments. Distortions and surface brightness variations in the shells of these large remnants also allow density variations and other characteristics of the ISM to be studied over the southern Galaxy.

It is interesting to note that, as these remnants become older and larger, they become more difficult to distinguish from the faint, patchy radio emission seen over the plane (see the 2.4-GHz survey images in Paper I). It is easy to imagine such remnants becoming fainter and more patchy, and eventually ‘disappearing’ into the ISM: i.e. losing their identity as individual remnants. It may be the case that much of the low surface brightness, patchy emission which clutters the plane out to the latitude limit of the survey (and presumably beyond) is produced by ancient supernovae with shells that are so evolved that they can no longer be distinguished as separate remnants.

The large candidate G310.5 – 3.5, described in Section 5.2.3 (see Fig. 16), is a case in point. Unlike many of the other large shells, which appear as thin, filamentary arcs, the shell of this candidate is faint, diffuse and patchy, with a noticeable gap on the eastern side. Perhaps this object is an old SNR, evolved to the point where the shock has essentially halted, which is slowly ‘diffusing’ into the ISM.

The distribution of these candidates along the plane is also of interest. Although they are probably old and relatively nearby, their distribution is far from isotropic; indeed, such candidates are detected over only a narrow range of Galactic longitudes, from about  $300^\circ$  to  $340^\circ$ . Furthermore, no similar objects have been reported from the Effelsberg 2.7-GHz survey (Reich et al. 1990), which covers the rest of the Galactic plane.

The histograms shown in Fig. 24 exhibit peaks within this longitude range, which are primarily due to the presence of these large SNR candidates. The fact that these objects appear over such a restricted range of longitudes strongly implies a general spatial correlation: i.e. these objects may all lie at a similar distance. Note that our largest candidate, G325 + 0, is  $18^\circ$  in angular diameter – which implies that such a grouping must be relatively close, probably no further than the Carina spiral arm. Some of these objects, such as G310.5 – 3.5 (Section 5.2.3), exhibits a polarized emission component. The vector orientations of the polarization across this remnant suggest low rotation measures, again implying that these objects must be relatively nearby.

If these objects are indeed associated with one another, one possibility is that their progenitor stars were all part of an association – an OB cluster, say. The fact that all of these SNR candidates appear large and old is broadly consistent with the idea of their progenitors being part of an OB association, since many of the stars in such clusters have similar lifetimes.

### 6.3 Pulsar associations

For the large remnants, looking for any pulsar associations would be a difficult task. As the candidates are of large angular size, many pulsars are often seen near the objects – for example, 16 pulsars (from the catalogue of Taylor, Manchester & Lyne 1993) can be seen in Fig. 15, which shows the candidates G304 + 0 and G304 + 2. That the candidates appear highly evolved also complicates matters, as any associated pulsar may have moved a considerable angular distance from its birthplace. Good distance estimates to these large candidates, coupled with pulsar proper motion studies, will doubtless be required to address these questions more fully.

The smaller remnant candidates perhaps hold more promise. Again consulting the catalogue of Taylor et al. (1993), we find only two pulsars present near any of these objects, namely the candidates G356.2 + 4.4 and G310.6 – 2.0. It is of interest to consider these briefly in more detail.

#### 6.3.1 G356.2 + 4.4

The pulsar B1717 – 29 is located approximately 20 arcmin to the south-east of the remnant candidate G356.2 + 4.4, and its position is marked on Fig. 11(a).

Any association between this pulsar and the remnant candidate must be considered extremely unlikely, chiefly because of the age of the pulsar. The shell of the candidate appears bright and well-defined, which is characteristic of younger remnants. This is inconsistent with the age of the pulsar, which was estimated by Taylor et al. (1993) to be  $1.3 \times 10^7$  yr.

### 6.3.2 G310.6–2.0

This case is possibly more interesting. Here, the pulsar B1358–63 is located near the geometric centre of the small candidate SNR G310.6–2.0 (the position of the pulsar is marked on Fig. 7). The spin-down age of this pulsar is estimated to be  $8 \times 10^5$  yr (Taylor et al. 1993).

Here, several possible interpretations are possible. First, the pulsar may be simply a chance superposition, unrelated to anything that we can identify from the 2.4-GHz survey images. Another possibility is that it is indeed related to the G310.6–2.0 candidate. This is somewhat unlikely, because G310.6–2.0 appears too bright for a remnant with an age of the order of  $10^6$  yr (that of the pulsar). Furthermore, we would expect the pulsar to have moved a greater angular distance from the geometric centre of G310.6–2.0 if this were the case.

We commented in Section 5.2.3 that the G310.6–2.0 candidate was superposed on the emission from another, much larger candidate SNR: G310.5–3.5. Fig. 16(a) shows both these objects in the same image. Note that this larger field shows no additional pulsars from the Taylor et al. (1993) catalogue. A further possibility is that the pulsar B1358–63 is related to the larger G310.5–3.5 candidate. This is a more attractive option, since the appearance of the large SNR candidate suggests that it is highly evolved – perhaps of the order of  $10^6$  yr old.

Finally, we note that the pulsar may have originated with the larger remnant, and that the bright shell emission identified as the SNR candidate G310.6–2.0 may be a result of the presence of the pulsar in this region of the shell.

## 7 FURTHER WORK

To investigate further the candidates presented here, and confirm them as supernova remnants, higher resolution observations at multiple frequencies are required. To this end, follow-up radio observations are under way with a number of instruments.

For the smaller objects, with diameters of about  $1^\circ$  and smaller, high-resolution, mosaiced images are being obtained with the Australia Telescope Compact Array (ATCA) at frequencies of 1.4 and 2.4 GHz. Additionally, the candidates to the north of  $\delta = -40^\circ$  are being imaged at 1.4 GHz with the Very Large Array (VLA).

Because of time constraints, it is impractical to image the larger objects with either the ATCA or the VLA. Instead, further Parkes observations are being sought for these objects.

Additionally, optical observations and X-ray data will further assist in the study of these objects.

## 8 CONCLUDING REMARKS

We have presented a list of 25 new SNR candidates distributed along the southern Galactic plane. Most of these remnants are of large angular size ( $\geq 20$  arcmin) – a class of remnant which has been poorly represented over the southern plane until now. The discovery of several candidates with angular sizes  $\approx 10^\circ$  is particularly interesting.

Future Galactic H I studies, such as the forthcoming Parkes multibeam survey, will help to establish kinematic distances to some of these SNRs.

## ACKNOWLEDGMENTS

The images presented in this paper were printed using the MIRIAD data reduction package. The University of Queensland's installation of MIRIAD is maintained remotely by the Australia Telescope National Facility.

## REFERENCES

- Bedford D. K., Elliott K. H., Ramsey B., 1984, MNRAS, 210, 693
- Beichman C. A., Neugebauer G., Habing H. J., Clegg P. E., Chester T. J., 1988, *IRAS Catalogue and Atlases, Version 2, Explanatory Supplement*, NASA Ref. Publ. 1190
- Berkhuijsen E. M., 1986, A&A, 166, 257
- Berkhuijsen E. M., Haslam C. G. T., Salter C. J., 1971, A&A, 14, 252
- Broadbent A., Osborne J. L., Haslam C. G. T., 1989, MNRAS, 237, 381
- Busser J. U., Egger R. J., Aschenbach B., 1995, IAU Circ. 6142
- Caswell J. L., Haynes R. F., 1987, A&A, 171, 261
- Dickel J. R., Sault R. J., Arendt R. G., Korista K. T., Matsui Y., 1988, ApJ, 330, 254
- Duncan A. R., Stewart R. T., Haynes R. F., Jones K. L., 1995, MNRAS, 277, 36 (Paper I)
- Egger R. J., Aschenbach B., 1995, A&A, 294, L25
- Fürst E., Reich W., Sofue Y., 1987, A&AS, 71, 63
- Gray A. D., 1994, MNRAS, 270, 861
- Green D. A., 1984, MNRAS, 209, 449
- Green D. A., 1988, Ap&SS, 148, 3
- Green D. A., 1995, A Catalogue of Galactic Supernova Remnants (1995 July version). Mullard Radio Astronomy Observatory, Cambridge (available over the World Wide Web at <http://www.mrao.cam.ac.uk/surveys/snrs/>)
- Gull T. R., Kirshner R. P., Parker R. A. R., 1977, ApJ, 215, L69
- Hughes J. P., Helfand D. J., Kahn S. M., 1984, ApJ, 281, L25
- Kesteven M. J., Caswell J. L., 1987, A&A, 183, 118
- Laval A., 1972, A&A, 19, 82
- McAdam W. B., Osborne J. L., Parkinson M. L., 1993, Nat, 361, 516
- Manchester R. N., 1987, A&A, 171, 205
- Meaburn J., Rovithis P., 1977, Ap&SS, 46, L7
- Meaburn J., Goudis C., Solomons N., Laspas V., 1991, A&A, 252, 291
- Milne D. K., Dickel J. R., 1975, Aust. J. Phys., 28, 209
- Perry C. L., Hill G., Christodoulou D. M., 1991, A&AS, 90, 195
- Reich W., Fürst E., Reich P., Reif K., 1990, A&AS, 85, 633
- Taylor J. H., Manchester R. N., Lyne A. G., 1993, ApJS, 88, 529
- Wright A. E., Griffith M. R., Burke B. F., Ekers R. D., 1994, ApJS, 91, 111